Published online 6 November 2017

Nucleic Acids Research, 2018, Vol. 46, No. 2 ***593–608***
doi: 10.1093/nar/gkx1052

Dynamic reorganization of open chromatin underlies diverse transcriptomes during spermatogenesis

So Maezawa[1,2], Masashi Yukawa[2,3], Kris G. Alavattam[1,2], Artem Barski[2,3] and Satoshi H. Namekawa[1,2,*]

[1]Division of Reproductive Sciences, Division of Developmental Biology, Perinatal Institute, Cincinnati Children's Hospital Medical Center, Cincinnati, OH 45229, USA, [2]Department of Pediatrics, University of Cincinnati College of Medicine, Cincinnati, OH 49267, USA and [3]Division of Allergy and Immunology, Division of Human Genetics, Cincinnati Children's Hospital Medical Center, Cincinnati, OH 45229, USA

Received August 30, 2017; Revised October 13, 2017; Editorial Decision October 16, 2017; Accepted November 02, 2017

ABSTRACT

During spermatogenesis, germ cells undergo massive cellular reconstruction and dynamic chromatin remodeling to facilitate highly diverse transcriptomes, which are required for the production of functional sperm. However, it remains unknown how germline chromatin is organized to promote the dynamic, complex transcriptomes of spermatogenesis. Here, using ATAC-seq, we establish the varied landscape of open chromatin during spermatogenesis. We identify the reorganization of accessible chromatin in intergenic and intronic regions during the mitosis-to-meiosis transition. During the transition, mitotic-type open chromatin is closed while the *de novo* formation of meiotic-type open chromatin takes place. Contrastingly, differentiation processes such as spermatogonial differentiation and the meiosis-to-postmeiosis transition involve chromatin closure without the *de novo* formation of accessible chromatin. In spermiogenesis, the germline-specific Polycomb protein SCML2 promotes the closure of open chromatin at autosomes for gene suppression. Paradoxically, we identify the massive *de novo* formation of accessible chromatin when the sex chromosomes undergo meiotic sex chromosome inactivation, and this is also mediated by SCML2. These results reveal meiotic sex chromosome inactivation as an active process for chromatin organization. Together, our results unravel the genome-wide, dynamic reorganization of open chromatin and reveal mechanisms that underlie diverse transcriptomes during spermatogenesis.

INTRODUCTION

The testis has the most diverse transcriptome, enriched with protein-coding and non-coding transcripts that are expressed in no other organs (1–3). Due to this diversity, the testis transcriptome is the most complex in comparison to the transcriptomes of other organs, even more complicated than that of the brain or cerebellum (3). This complexity is driven, in large part, by the expression of vast portions of the genome that are largely dormant in somatic cell lineages. Furthermore, this unique expression is functional, shaping the unique purpose of the germline to propagate life. However, it remains unknown how germ-cell chromatin is organized to facilitate the diverse transcriptomes of spermatogenesis. Elucidation of chromatin organization during spermatogenesis will unravel how extensive tracts of the genome, dormant in most cells, are poised for functions that ensure the continuity of life.

To prepare functional sperm, germ cells undergo progressive morphological changes and differentiation beginning in a stem cell phase (4–7). While some male germ cells self-renew to support a stem cell pool during adult life, others differentiate, undergoing serial mitotic proliferation that results in massive numbers of germ cells. Then, upon entry into meiosis, male germ cells begin a process of differentiation to become haploid spermatids. The differentiation processes that comprise spermatogenesis are accompanied by large-scale events in cellular reconstruction and chromatin remodeling (5–7).

A growing literature indicates that genome-wide gene expression is altered by the activation of germline-specific genes during meiosis, a process that continues in postmeiotic spermatids (8–18). These genes, numbering several thousand, form a class termed late spermatogenesis genes (14,15). A separate class of genes, numbering several thousand and expressed in somatic lineages and the progenitors of spermatogenic cells, is largely suppressed during meiosis and in postmeiotic spermatids (14,15). These genes, termed somatic/progenitor genes, are commonly expressed in cells

*To whom correspondence should be addressed. Tel: +1 513 803 1377; Fax: +1 513 803 1160; Email: satoshi.namekawa@cchmc.org

undergoing mitotic proliferation. Concurrent with changes in gene expression, chromatin immunoprecipitation with sequencing (ChIP-seq) assays reveal a genome-wide alteration of histone tail modifications during spermatogenesis (15,19). However, in the context of such changes, a central question remains: How are the dynamic gene expression changes of spermatogenesis regulated at the chromatin level?

To determine the genome-wide organization of chromatin at nucleosome resolution, we establish the landscape of open chromatin during spermatogenesis through the Assay for Transposase-Accessible Chromatin with high-throughput sequencing (ATAC-seq) (20). ATAC-seq detects and details regions of open chromatin based on their accessibility to the Tn5 transposase. Our results unravel the dynamic reorganization of accessible chromatin in intergenic and intronic regions during the mitosis-to-meiosis transition. In addition to chromatin reorganization at autosomes, we also identify the *de novo* formation of accessible chromatin at the sex chromosomes during meiosis, when the unsynapsed X and Y chromosomes undergo meiotic sex chromosome inactivation (MSCI). We identify mechanisms that underlie the accessibility of chromatin. We show that the germline-specific Polycomb protein SCML2, which suppresses somatic/progenitor genes in the later stages of spermatogenesis (14), has distinct functions in the regulation of open chromatin both at autosomes and sex chromosomes. These results reveal mechanisms for the organization of germline chromatin associated with diverse transcriptomes during spermatogenesis.

MATERIALS AND METHODS

Animals

Scml2-KO mice were previously reported (14).

Immunohistochemistry

For preparation of testicular paraffin blocks, testes were fixed with 4% paraformaldehyde (PFA) at 4°C overnight. Testes were dehydrated and embedded in paraffin. Paraffin sections at 7 μm thick were deparaffinized and autoclaved in Target Retrieval Solution (DAKO) at 121°C for 10 min. The sections were blocked with Blocking One Histo (Nacalai USA) for 1 h at room temperature, and then incubated with primary antibodies (rabbit anti-PLZF antibody from Santa Cruz, and goat anti-KIT antibody from R&D Systems) at 4°C overnight. The resulting signals were detected by incubation with secondary antibodies conjugated to Alexa 555 or Alexa 647 (Thermo Fisher Scientific). Sections were counterstained with DAPI. Images were obtained by confocal laser scanning microscope (A1R, Nikon) and processed with NIS-Elements (Nikon), and Image J (National Institutes of Health).

Germ cell fractionation

Spermatogonia were isolated as described previously (14) and collected from C57BL/6N mice aged 6–8 days. Testes were collected in a 24-well plate of Dulbecco's Modified Eagle Medium (DMEM) supplemented with GlutaMax (Thermo Fisher Scientific), non-essential amino acids (NEAA) (Thermo Fisher Scientific), and penicillin and streptomycin (Thermo Fisher Scientific). After removing the *tunica albuginea* membrane, testes were digested with collagenase (1 mg/ml) at 34°C for 20 min to remove interstitial cells and then centrifuged at 188 × *g* for 5 min. Tubules were washed with the medium and then digested with trypsin (2.5 mg/ml) at 34°C for 20 min to obtain a single cell suspension. Cells were filtered with a 40-μm strainer to remove Sertoli cells, and the cell suspension was plated in a 24-well plate for 1 h in the medium supplemented with 10% fetal bovine serum, which promotes adhesion of remaining somatic cells. Cells were washed with magnetic cell-sorting (MACS) buffer (PBS supplemented with 0.5% BSA and 5 mM EDTA) and incubated with CD117 (KIT) MicroBeads (Miltenyi Biotec) on ice for 20 min. Cells were washed and resuspended with MACS buffer, and filtered with a 40-μm strainer. Cells were separated by autoMACS Pro Separator (Miltenyi Biotec) with the program 'possel'. Cells in the flow-through fraction were washed with MACS buffer and incubated with CD90.2 (THY1) MicroBeads (Miltenyi Biotec) on ice for 20 min. Cells were washed and resuspended with MACS buffer and filtered with a 40-μm strainer. Cells were separated by autoMACS Pro Separator (Miltenyi Biotec) with the program 'posseld'. The purity of islolated spermtogonia was confirmed by immunostaining (Supplementary Figure S1A and B). More than 95% purity was confirmed for all purifications of $THY1^+$ and KIT^+ spermatogonia.

Pachytene spermatocytes (PS) and round spermatids (RS) were isolated via BSA gravity sedimentation as previously described (21) and collected from C57BL/6N mice aged 90–120 days. Purity was confirmed by nuclear staining with Hoechst 33342 using fluorescence microscopy (Supplementary Figure S1C and D). More than 90% purity was confirmed for all purifications of PS and RS.

Immunocytochemistry

Cells ($1–3 \times 10^5$) were washed with germline stem (GS) cell culture medium (14), and then resuspended with 10 μl of the medium. Cell suspension was spotted on a CELLView Cell Culture Dish (greiner bio-one), which was pre-coated with 0.01% Poly-L-lysine solution (Sigma), and incubated at 34°C for 20 min to promote adhesion. Cells were fixed with 4% PFA for 20 min at 34°C, permeabilized with 0.05% TritonX-100 for 10 min at room temperature, blocked with Blocking One Histo (Nacalai USA) for 20 min at room temperature, and then incubated with primary antibodies (rabbit anti-PLZF antibody from Santa Cruz, goat anti-KIT antibody from R&D Systems and anti-GCNA antibody from Abcam) at 4°C over night. The resulting signals were detected by incubation with secondary antibodies conjugated to fluorophores (Thermo Fisher, Biotium or Jackson ImmunoResearch). Nuclei were counterstained with DAPI. Images were obtained by an ECLIPSE Ti-E microscope (Nikon) equipped with a Zyla 5.5 sCMOS camera (Andor Technology) and 100× CFI Apochromat TIRF oil immersion objective NA 1.4 (Nikon), and processed with NIS-Elements (Nikon) and Image J.

ATAC-seq library preparation and sequencing

ATAC-seq libraries were prepared as previously described (20). Approximately 500 000 THY1$^+$ or KIT$^+$ spermatogonia, 250 000 PS and 1 000 000 RS were used. Briefly, samples were lysed in 50 μl of lysis buffer (10 mM Tris–HCl (pH 7.4), 10 mM NaCl, 3 mM $MgCl_2$ and 0.1% NP-40). Immediately after lysis, nuclei were spun at 500 × *g* for 5 min to remove the supernatant. Nuclei were then incubated with Tn5 transposase and tagmentation buffer (Illumina) at 37°C for 30 min. After tagmentation, the transposed DNA was purified with a MinElute kit (Qiagen). Polymerase chain reaction (PCR) was performed to amplify the library using the following conditions: 72°C for 5 min; 98°C for 30 s; thermocycling at 98°C for 10 s, 63°C for 30 s and 72°C for 1 min; and 72°C for 5 min as the final elongation. qPCR was used to estimate the number of additional cycles needed to generate products at 25% saturation. Typically, two to five additional PCR cycles were added to the initial set of five cycles. The library was purified by AMPure XP beads (Beckman). Size selection of library pools was achieved by agarose gel electrophoresis, excising gel slices in the 250- to 500-bp range. Pools purified from gel slices were analyzed on an Agilent Bioanalyzer, and 75-bp single-read sequencing was performed using an Illumina HiSeq 2500 platform per standard operating procedures.

Code availability: ChIP-seq and RNA-seq data

RNA-seq data from THY1$^+$ spermatogonia, PS and RS were downloaded from the Gene Expression Omnibus (accession number: GSE55060) (14). ChIP-seq data for RNAPII in GS cells were downloaded from the Gene Expression Omnibus (accession number: GSE69949) (15). ChIP-seq data for RNAPII in PS and RS were downloaded from the Gene Expression Omnibus (accession number: GSE45441) (22). ChIP-seq data for DMC1-ssDNA were downloaded from the Gene Expression Omnibus (accession number: GSE75419) (23). Affinity-seq data for PRDM9-binding sites were downloaded from the Gene Expression Omnibus (accession number: GSE61613) (24). ChIP-seq data for H3K4me3, H3K4me2 and H3K27me3, and RNA-seq data from KIT$^+$ spermatogonia were downloaded from the Gene Expression Omnibus (accession number: GSE59502) (manuscript submitted). ChIP-seq data for H3K4me3 and H3K27me3 from sperm were downloaded from the Gene Expression Omnibus (accession number: GSE42629) (25).

ATAC-seq and ChIP-seq data analysis

Data analyses for ATAC-seq and ChIP-seq were performed in the Wardrobe Experiment Management System (https://code.google.com/p/genome-tools/, (26)). Briefly, reads were aligned to the mouse genome (mm10) with Bowtie (version 1.0.0 (27)) with a maximum of one allowed error in a sequence and no more than one hit allowed, assigned to RefSeq genes (or isoforms) using the Wardrobe algorithm, and displayed on a local mirror of the UCSC genome browser as coverage. We analyzed the confidence peaks present in one of the representative replicates for analyses. ATAC-seq peaks and ChIP-seq peaks for H3K27me3, H3K4me2, H3K4me3 and RNAPII were identified using MACS2 (version 2.1.0.20140616 (28)). MACS2 was used to estimate fragment size and to find islands of enrichment, and with a *q*-value threshold <0.2. For data visualization, data were uploaded to UCSC genome browser, and fragment coverage was determined by estimated fragment sizes from MACS2 output. MAnorm, software designed for quantitative comparison of ChIP-seq datasets (29), was applied to compare the genome-wide ATAC-seq peaks among stages in spermatogenesis. Unique peaks were defined using the following criteria: (i) defined as 'unique' by the MAnorm algorithm, (ii) P-value < 0.01 and (iii) raw read counts of unique peaks > 10. Common peaks between two stages were defined using the following criteria: (i) defined as 'common' by the MAnorm algorithm and (ii) raw read counts for both stages >10. Average tag density profiles were calculated around RefSeq transcription start sites (TSSs) for gene sets of somatic/progenitor genes, late spermatogenesis genes, constitutive active genes and constitutive inactive genes as described previously (15). Resulting graphs were smoothed in 200-bp windows. Enrichment levels for ChIP-seq experiments were calculated for 4-kb windows around promoter regions of RefSeq genes (±2 kb surrounding TSSs). To normalize tag values, read counts were multiplied by 1 000 000 and then divided by the total number of reads at each nucleotide position. Total amounts of tag values in promoter regions were calculated as enrichment. MEME-ChIP (30) was used for motif discovery as described in the text. For all motif analyses, only peak regions (±250 bp from the peak summit) outside ±1 kb of TSSs (termed distal peaks) were used, and a maximum of 3000 peak regions from the lowest P-values (P < 0.01) were chosen via MAnorm analysis. These sequences were extracted using the Table Browser (31). Relative locations of peak regions were analyzed using GREAT with default settings (32).

RNA-seq data analysis

Data analysis for RNA-seq was performed in the Wardrobe Experiment Management System. (26). FASTQ files from the Illumina pipeline were aligned via the Spliced Transcripts Alignment to a Reference (STAR) software (version STAR_2.4.2a) (33) with the following parameters: –outFilterMultimapNmax 1 –outFilterMismatchNmax 2 (to see the full manual, go to this STAR GitHub page: https://github.com/alexdobin/STAR/blob/master/doc/STARmanual.pdf?raw=true). RefSeq annotation from the UCSC genome browser (11/2012) (34) for the mm10 genome was used. The –outFilterMultimapNmax parameter was used to allow unique alignment only, and the –outFilterMismatchNmax parameter was used to allow a maximum of only two errors. All reads from resulting bam files were split for related isoforms with respect to RefSeq annotation. Then, the EM algorithm was used to estimate appropriate numbers of reads for each isoform (26). To estimate differences between experiments, the DESeq2 package (35) was used.

RESULTS

The accessible chromatin landscape in spermatogenesis

During spermatogenesis, the nuclear architecture of germ cells undergoes extensive remodeling. Undifferentiated spermatogonia progress into and through mitotic differentiation, meiosis and postmeiotic differentiation to finally produce haploid sperm (Figure 1A). This progression through spermatogenesis is discernible by the changing, stage-specific organization of heterochromatin. In undifferentiated spermatogonia, detected with the marker ZBTB16 (also known as PLZF), DAPI-discernible heterochromatin is largely absent and the nucleus is almost uniformly stained with DAPI (Figure 1B, #1), suggesting that the nuclei of undifferentiated spermatogonia are largely euchromatic. In differentiating spermatogonia, detected with the marker KIT (also known as c-Kit), several clusters of DAPI-dense heterochromatin become discernible (Figure 1B, #2). After entry into meiosis, more heterochromatin clusters are observed in PS, and the overall chromatin organization is distinct from previous mitotic stages (Figure 1B, #3). Following meiotic division, the heterochromatin of RS is clustered in a central region of the nucleus to form a chromocenter (Figure 1B, #4). Because heterochromatin organization (i.e. closed chromatin) changes through progressive stages of spermatogenesis, we anticipated that open chromatin is also altered during spermatogenesis to ensure the genome-wide gene expression changes of spermatogenesis.

To determine the genome-wide chromatin organization of spermatogenesis at nucleosome resolution, we performed ATAC-seq, detecting genomic regions of Tn5 transposase-accessible chromatin (20). We analyzed four representative stages of spermatogenesis: THY1$^+$ undifferentiated spermatogonia, which contain spermatogonial stem cells and progenitor cells; KIT$^+$ differentiating spermatogonia from postnatal day 7 (P7) testes; purified PS undergoing meiosis; and postmeiotic RS from adult testes (Figure 1A). We used P7 spermatogonia because our optimized protocol allows us to isolate highly purified spermatogonia at this stage without contamination from differentiated germ cells (14) (Supplementary Figure S1). We carried out ATAC-seq for two independent biological replicates to confirm that the signals from ATAC-seq are consistently detected at the same genomic loci (Supplementary Figure S2A) and are highly correlated between the replicates (Supplementary Figure S2B). The total number of ATAC peaks detected with MACS2, a peak detection program (28), decreased from THY1$^+$ spermatogonia to RS (Figure 1C). During this process, the number of ATAC peaks greatly decreased in intergenic and intron regions (48 068, 25 585, 31 072, 17 220 from THY1$^+$ to RS in intergenic regions; 53 605, 27 975, 26 515, 13 753 from THY1$^+$ to RS in intron regions), yet the number of ATAC peaks in promoters underwent only a modest decrease (43 298, 33 704, 28 868, 27 927 from THY1$^+$ to RS in promoters). From a chromosome-wide view, ATAC signals were enriched at gene-rich regions throughout spermatogenesis (Supplementary Figure S2C). Overall, the enrichment of accessible chromatin inversely correlates with the presence of DAPI-discernible heterochromatin, and chromatin accessibility gradually decreases over the course of spermatogenic differentiation.

Notably, ATAC peaks at the sex chromosomes greatly increased in PS, when sex chromosomes undergo the transcriptional silencing of MSCI (Figure 1C and D). At this stage, ATAC signals were increased at largely intergenic and intronic regions of the sex chromosomes (Figure 1C). RNA-seq analysis confirmed the transcriptional suppression of the sex chromosomes in spite of PS-specific chromatin opening (Figure 1E). After meiotic divisions, ATAC peaks at the sex chromosomes were diminished in RS (Figure 1C and D), where chromosome-wide silencing of the sex chromosomes is largely maintained (11,36) (Figure 1E). These results suggest that, due to MSCI, the chromatin accessibility of the sex chromosomes is differentially regulated from that of autosomes during late spermatogenesis.

To determine whether the chromatin accessibility detected by ATAC-seq is associated with gene expression during spermatogenesis, we analyzed the enrichment of ATAC signals around TSSs of RefSeq genes as detected by RNA-seq (14). Although the enrichment of ATAC signals typically correlates with gene expression during spermatogenesis, there are a large number of unexpressed genes enriched with ATAC signals (the dashed rectangle in Figure 2A and Supplementary Figure S3). Genes with this feature become evident in PS and RS, suggesting that gene expression is not necessarily predictive of accessible chromatin during late spermatogenesis. Next, we examined the correlation between ATAC signals, active histone epigenetic modifications and RNA polymerase II (RNAPII). Genome-wide, TSSs enriched with ATAC signals were highly correlated with TSSs enriched with the active marks H3K4me3 and H3K4me2, and RNAPII (Figure 2A and Supplementary Figure S3).

In contrast, the repressive mark H3K27me3 showed a characteristic distribution during spermatogenesis: while many TSSs enriched with ATAC signals were devoid of H3K27me3, we observed one group of TSSs enriched with ATAC signals and H3K27me3 (Figure 2A). These TSSs feature bivalent domains that retain both repressive H3K27me3 and active H3K4me2/3. During spermatogenesis, most of the TSSs enriched with H3K27me3 form bivalent domains (Maezawa *et al.*, submitted), which are considered to be a molecular hallmark of developmental potential (37–39). Our recent study defined two classes of bivalent domain genes. Class I bivalent domains comprise somatic developmental regulator genes that are not expressed in spermatogenesis, and Class I bivalent domains are maintained throughout spermatogenesis (19,25,40–43). Class II bivalent domains comprise somatic and progenitor genes that are silenced in late spermatogenesis, are not initially bivalent in spermatogonia, and are later established during meiotic prophase (15) (Maezawa *et al.*, submitted). Genes with these two classes of bivalent domains are largely repressed in gene expression but are modestly enriched with ATAC signals (Figure 2B). These results indicate that TSSs with bivalent domains have repressed gene expression yet retain accessible chromatin, supporting the notion that these genes can be reactivated after fertilization to recover totipotency (15,44,45). This feature also explains why there is a large

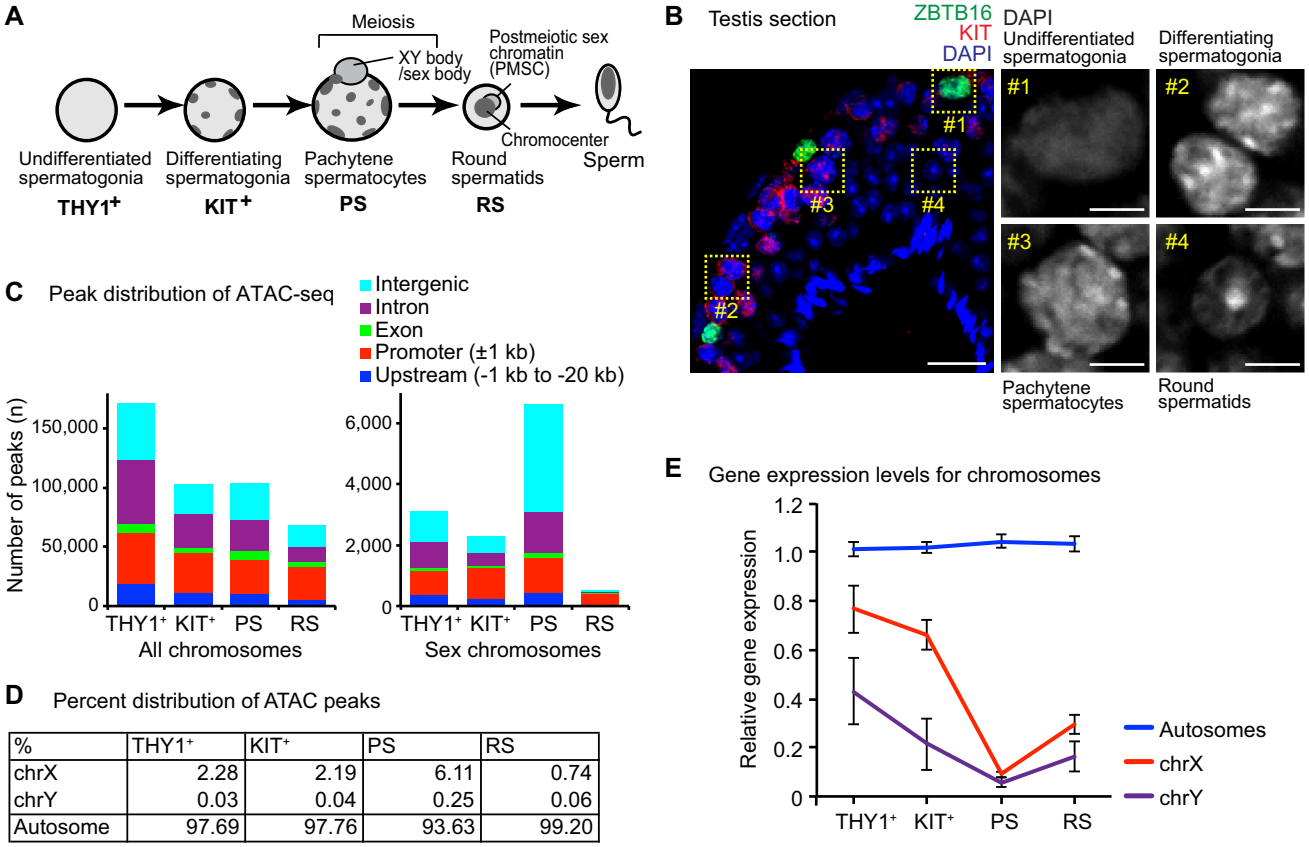

%	THY1+	KIT+	PS	RS
chrX	2.28	2.19	6.11	0.74
chrY	0.03	0.04	0.25	0.06
Autosome	97.69	97.76	93.63	99.20

Figure 1. Global characteristics of accessible chromatin during spermatogenesis. (**A**) Schematic of spermatogenesis and the four representative stages analyzed in this study. (**B**) Immunostaining of testicular paraffin sections with anti-ZBTB16 and anti-KIT antibodies. Slides were counterstained with DAPI. Images were acquired with a confocal microscope. Regions bordered by dashed yellow squares are magnified in the right panels. Bar in left panel: 20 μm; bars in right panels: 5 μm. (**C**) Numbers of ATAC peaks during spermatogenesis detected by MACS2 analysis. The analysis was performed for all chromosomes (left) and the sex chromosomes (right). The genomic distribution of each peak is shown with colored bars. (**D**) Percent distribution of ATAC peaks at the X and Y chromosomes, and autosomes. (**E**) Relative gene expression levels of the X and Y chromosomes, and autosomes. The mean expression level of each chromosome was normalized to the mean of all genes as 1.

number of unexpressed genes enriched with ATAC signals (Figure 2A).

Next, we sought to determine whether the chromatin states of RS are retained prior to fertilization. We analyzed published ChIP-seq data in sperm for H3K27me3 and H3K4me3—histone modifications that are retained in TSSs and not replaced with protamines (25)—along with ATAC signals at these sites in RS. In sperm, we found three classes of promoters dependent on the accumulation status of H3K27me3 and H3K4me3 (Figure 2C). The first class is depleted of H3K4me3 (enrichment of H3K4me3 < 1; blue area in Figure 2C), the second class is enriched with H3K4me3 but not H3K27me3 (H3K4me3 > 1, H3K27me3 < 1; pink area in Figure 2C) and the third class is enriched with both H3K4me3 and H3K27me3 (H3K4me3 > 1, H3K27me3 > 1; green area in Figure 2C), thereby containing bivalent promoters. ATAC signals in RS were enriched at the second and third classes of promoters (right-hand panel in Figure 2C). Thus, we conclude that, from RS to sperm, open chromatin is maintained on H3K4me3-enriched promoters.

Dynamic change of accessible chromatin during the mitosis-to-meiosis transition

To elucidate how chromatin accessibility changes during spermatogenesis, we examined the dynamics of chromatin accessibility at the transitions from one stage of spermatogenesis into the next. For the quantitative analyses of ATAC peaks at each transition, we used MAnorm, peak analysis software that is more stringent than MACS2, to quantitatively compare peaks derived from two pairwise next-generation sequencing datasets (29). Between ATAC peaks from THY1$^+$ and KIT$^+$ spermatogonia, a large fraction were defined as common and peaks unique to KIT$^+$ were scarce (Figure 3A). This result suggests that most peaks in spermatogonia are present early in the THY1$^+$ stage, and accessible chromatin unique to THY1$^+$ is closed as spermatogonia differentiate from THY1$^+$ to KIT$^+$. Furthermore, the *de novo* formation of accessible chromatin is scarce during spermatogonial differentiation from THY1$^+$ to KIT$^+$.

MAnorm analysis between KIT$^+$ spermatogonia and PS revealed a dynamic change in chromatin accessibility during the mitosis-to-meiosis transition. Between ATAC peaks from KIT$^+$ spermatogonia and PS, 32 158 peaks were de-

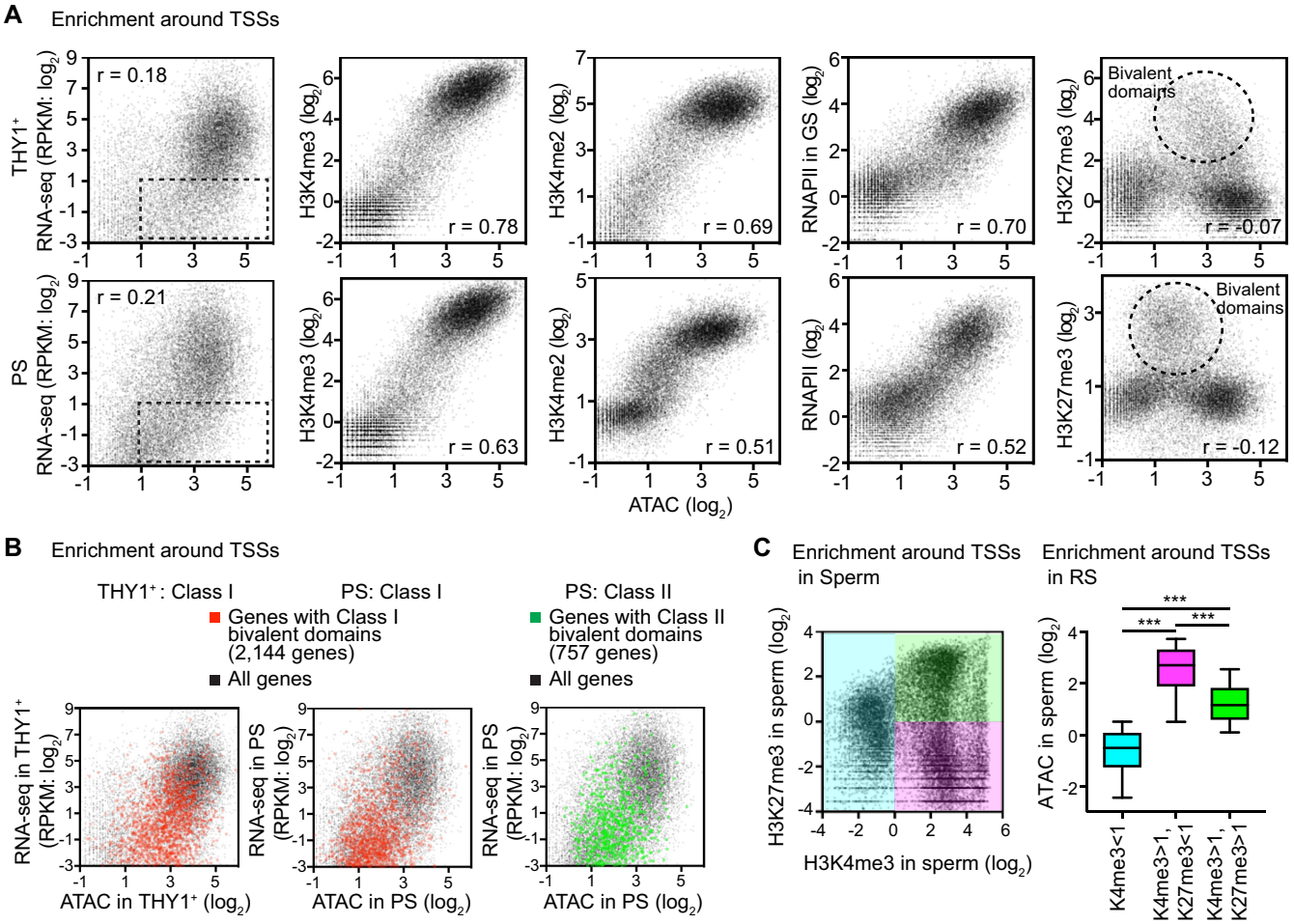

Figure 2. Accessible chromatin in relation to gene expression and histone modifications during spermatogenesis. (**A**) Enrichment analysis of accessible chromatin (ATAC-seq) around TSSs (±2 kb) with gene expression (RNA-seq), H3K4me3, H3K4me2, RNAPII and H3K27me3 (ChIP-seq). Upper panels show the correlation in THY1$^+$ spermatogonia; bottom panels show the correlation in PS. Pearson correlation values are shown. ATAC-seq of THY1$^+$ spermatogonia was analyzed through the use of RNAPII in cultured GS cells (15). In the RNA-seq panels, dashed rectangles represent the genes enriched with ATAC signals (ATAC-seq enrichment > 2) that lack gene expression (RNA-seq: RPKM < 2) (**B**) Enrichment analysis of accessible chromatin (ATAC-seq) with H3K27me3 (ChIP-seq) around TSSs (±2 kb) for each class of bivalent domains. (**C**) Enrichment analysis of H3K27me3 and H3K4me3 around TSSs (±2 kb) in sperm (left panel). Enrichment analysis of RS ATAC signals at the classes of TSSs (±2 kb) defined in the left panel (right panel). *** $P <$ 0.0001, Mann–Whitney U test.

fined as unique to KIT$^+$, 28 796 peaks were defined as unique to PS and 19 594 peaks were common to both KIT$^+$ and PS (Figure 3A). This result suggests that accessible chromatin in KIT$^+$ spermatogonia are largely closed prior to meiosis, and *de novo* formation of accessible chromatin takes place in meiotic prophase. These changes occurred mostly in intergenic and intronic regions, while accessible chromatin in promoter regions was relatively stable during the mitosis-to-meiosis transition. We confirmed the dynamic change in chromatin accessibility of the mitosis-to-meiosis transition by comparing THY1$^+$ spermatogonia and PS (Supplementary Figure S4). Since there is a massive change in transcription during the mitosis-to-meiosis transition, it is conceivable that the chromatin accessibility of regulatory elements in intergenic and intronic regions is reorganized at the transition to facilitate the change in transcription.

Furthermore, we found that chromatin accessibility is largely reduced during the divisions and differentiation of meiotic PS into postmeiotic RS. By comparing ATAC peaks between PS and RS, we identified 13 424 peaks unique to PS and 27 593 peaks common to both PS and RS. However, we found only 1524 peaks unique to RS, indicating that 65% of accessible chromatin is maintained after meiotic cell divisions and the remaining 35% is closed off (Figure 3A). During this step, accessible chromatin in promoter regions is relatively stable compared to chromatin in other regions.

Taken together, our analysis reveal massive reprogramming and *de novo* formation of accessible chromatin in intergenic and intronic regions during the mitosis-to-meiosis transition. On the other hand, during spermatogonial differentiation (THY1$^+$ to KIT$^+$) and the meiosis-to-postmeiosis transition (PS to RS), open chromatin tends to close without *de novo* formation of accessible chromatin.

During meiosis, recombination between homologous chromosomes is an essential chromatin event that facilitates genetic diversity in offspring. Because recombination occurs through the leptotene to zygotene stages of meiotic

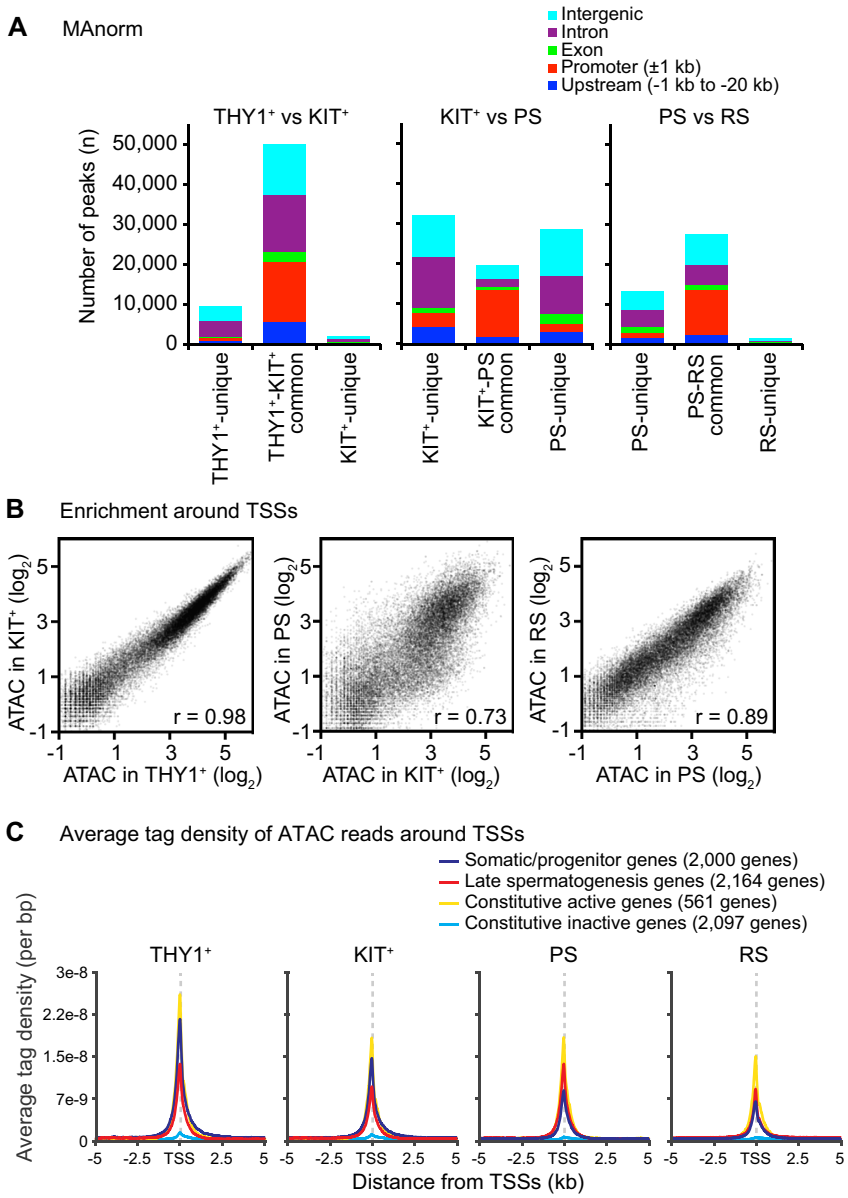

Figure 3. Dynamic changes in accessible chromatin during spermatogenesis. (**A**) MAnorm analysis of ATAC peaks at each transition of spermatogenesis. The genomic distribution of each peak is shown with colored bars. (**B**) Enrichment analysis of accessible chromatin (ATAC-seq) around TSSs (±2 kb) at each transition during spermatogenesis. Pearson correlation values are shown. (**C**) Average tag density of ATAC-seq reads around TSSs (±5 kb) for the indicated gene sets.

prophase, it is possible that chromatin accessibility in PS is associated with the remnants of recombination hotspots. In previous genome-scale analyses, meiotic recombination hotspots were detected by the presence of single-stranded DNA (ssDNA) bound to the meiosis-specific recombinase DMC1 (46) and also by PRDM9-binding sites, which are major determinants of meiotic recombination (24). To determine the relationship between sites of accessible chromatin and recombination hotspots, we analyzed our ATAC-seq data along with two published datasets: ssDNA sequencing data that detects DMC1-bound ssDNA at DSB ends (23), and affinity sequencing data that detects PRDM9-binding sites from *in vitro* purified DNA (24). For the most part, the regions of DMC1-bound ssDNA and PRDM9-binding sites were in intergenic and intronic regions; however, in KIT$^+$ spermatogonia and PS, we did not observe a large overlap between the regions of DMC1-bound ssDNA and accessible chromatin, nor did we observe a large overlap between PRDM9-binding sites and accessible chromatin (Supplementary Figure S5A and B). The regions of DMC1-bound ssDNA and PRDM9-binding sites were largely devoid of ATAC signals in KIT$^+$ spermatogonia and PS (Supplementary Figure S5C). Notably, the peaks of DMC1-bound ssDNA and PRDM9-binding sites overlap (Supplementary Figure S5C). Although we were not able to perform ATAC-seq of the spermatocytes in the leptotene and zygotene stages of meiotic prophase, which are undergoing initial and intermediate events in mei-

otic recombination, it is possible that DMC1-bound ssDNA and PRDM9-binding sites are temporarily regulated in the leptotene and zygotene stages. These results suggest that transposase-accessible chromatin established in PS is associated with unique gene expression rather than the remnants of recombination hotspots.

To further elucidate the varieties of accessible chromatin in spermatogenesis, we compared chromatin accessibility around TSSs between two stages through scatter plots of ATAC-seq read enrichment. Consistent with MAnorm analysis, chromatin accessibility around TSSs during spermatogonial differentiation (THY1$^+$ to KIT$^+$) and the meiosis-to-postmeiosis transition (PS to RS) were highly correlated (Figure 3B). The mitosis-to-meiosis transition (KIT$^+$ to PS) evinced a decreased, yet still high, correlation compared to the other transitions (Figure 3B), suggesting a moderate change in chromatin accessibility. Therefore, in addition to a change in chromatin accessibility in intergenic and intronic regions, there is a change around TSSs during the mitosis-to-meiosis transition, when a broad and dynamic change in transcription takes place.

Next, we sought to understand how chromatin accessibility around TSSs regulates the expression of stage-specific genes in spermatogenesis. We analyzed the chromatin accessibility around TSSs of somatic/progenitor genes (2000 genes that are active in spermatogonia but are suppressed in PS and RS by at least a 4-fold change) and late spermatogenesis genes (2164 genes that are unexpressed or expressed at a low level in spermatogonia, but are active in PS and RS by at least a 4-fold change). Somatic/progenitor genes retain a high level of chromatin accessibility around TSSs in THY1$^+$ and KIT$^+$ spermatogonia, and maintain a relatively high level of chromatin accessibility in meiotic PS and post-meiotic RS (Figure 3C). Interestingly, late spermatogenesis genes have a high level of chromatin accessibility around TSSs in THY1$^+$ and KIT$^+$ spermatogonia prior to activation (Figure 3C). Therefore, chromatin accessibility around the TSSs of both gene sets was largely maintained throughout spermatogenesis. This raises the possibility that chromatin accessibility in regulatory regions is dynamically reprogrammed to ensure the change in gene expression during the mitosis-to-meiosis transition.

Identification of distal gene regulatory regions during spermatogenesis

To determine the distal regulatory regions outside of TSSs, we analyzed the gain or loss of distal ATAC peaks located outside ±1 kb of TSSs (defined as 'distal ATAC peaks' hereafter). Because of the significant change in chromatin accessibility during the mitosis-to-meiosis transition, we focused our investigations on MAnorm results between KIT$^+$ spermatogonia and PS. Among the total distal ATAC peaks identified by MAnorm analysis, 7527 peaks were found to neighbor somatic/progenitor genes (i.e. the genes closest to these peaks are somatic/progenitor genes) and these peaks were enriched with KIT$^+$-unique peaks (Figure 4A). On the other hand, 5773 peaks were found to neighbor late spermatogenesis genes, and these peaks were enriched with PS-unique peaks (Figure 4A). To further verify the relationship between distal ATAC peaks and stage-specific gene expression, we performed hypergeometric probability tests with stringent criteria (>2-fold enrichment, P-value $< 1 \times 10^{-5}$). We confirmed that peaks unique to KIT$^+$ spermatogonia are significantly enriched in somatic/progenitor genes (1502 peaks, P-value $= 2 \times 10^{-42}$, hypergeometric probability test), and peaks unique to PS are significantly enriched in late spermatogenesis genes (864 peaks, P-value $= 2 \times 10^{-10}$, hypergeometric probability test) (Figure 4B). These results suggest that distal ATAC peaks are associated with stage-specific gene expression during the mitosis-to-meiosis transition.

In distal regulatory regions, accessible chromatin often contains transcription factor (TF)-binding sites (20,47). Therefore, we hypothesized that distal accessible chromatin harbors TF-binding motifs that facilitate the unique gene expression programs of spermatogenesis. By using the motif analysis program MEME-ChIP (48), we identified consensus motifs similar to known TF-binding motifs in distal accessible chromatin. These motifs include those unique to KIT$^+$ spermatogonia and those unique to PS (Figure 4C). Among the accessible chromatin unique to KIT$^+$, the TF-binding motif with the lowest E-value (E-value $= 4.8 \times 10^{-57}$, expected value from the MEME expectation maximization algorithm) (49) contained motifs for SOX10. SOX10 is an SRY-related HMG box (SOX) family TF implicated in the male differentiation of embryonic gonads (50), but the function of SOX10 in spermatogonia remains undetermined. Consistent with this finding, a similar SOX10 motif was found in differential methylated regions (DMRs), tracts of hypo-methylated DNA in spermatogonia that are hyper-methylated in sperm (51). The motif with the second lowest E-value (E-value $= 1.5 \times 10^{-32}$) contains a common binding motif for FOS, FOSL2 and JUND. These factors hold potential to promote the cell proliferation of KIT$^+$ spermatogonia, as the FOS family of transcription factors (FOS, FOSL2) are known to work with JUN family members (JUND) for cell proliferation (52). RNA-seq analysis revealed that these TFs are highly expressed in THY1$^+$ and KIT$^+$ spermatogonia (Supplementary Figure S6A). We also identified other consensus motifs, including NR5a2, a TF implicated in germ cell development (53) and the retinoid receptors RXRA and RXRB, which are binding targets for retinoic acids and essential for spermatogonia (54). RNA-seq analysis revealed that expression of these factors tends to be high in KIT$^+$ spermatogonia (Supplementary Figure S6A). Therefore, in KIT$^+$ spermatogonia, distal accessible chromatin harbors regulatory elements that are related to spermatogonial functions.

During our analyses of TF motifs found in accessible chromatin unique to PS, we identified relatively long and common consensus sequences (14–30 nt in length; Figure 4C). The sequence with the lowest E-value (E-value $= 3.2 \times 10^{-220}$) contains the motif CCAAT(ATTGG), a binding site for Nuclear Factor Y (NFYA and NFYB). Since NFYA and NFYB regulate meiosis-specific expression of *Miwi* (55), this motif is likely to be involved in meiosis-specific gene regulation. Furthermore, we identified motifs containing binding sites for POU family TFs that have important functions in spermatogenesis: POU3F1 (also known as Oct6) is required for spermatogonial stem cells (56), while POU5F2 (also known as Sprm-1) is expressed imme-

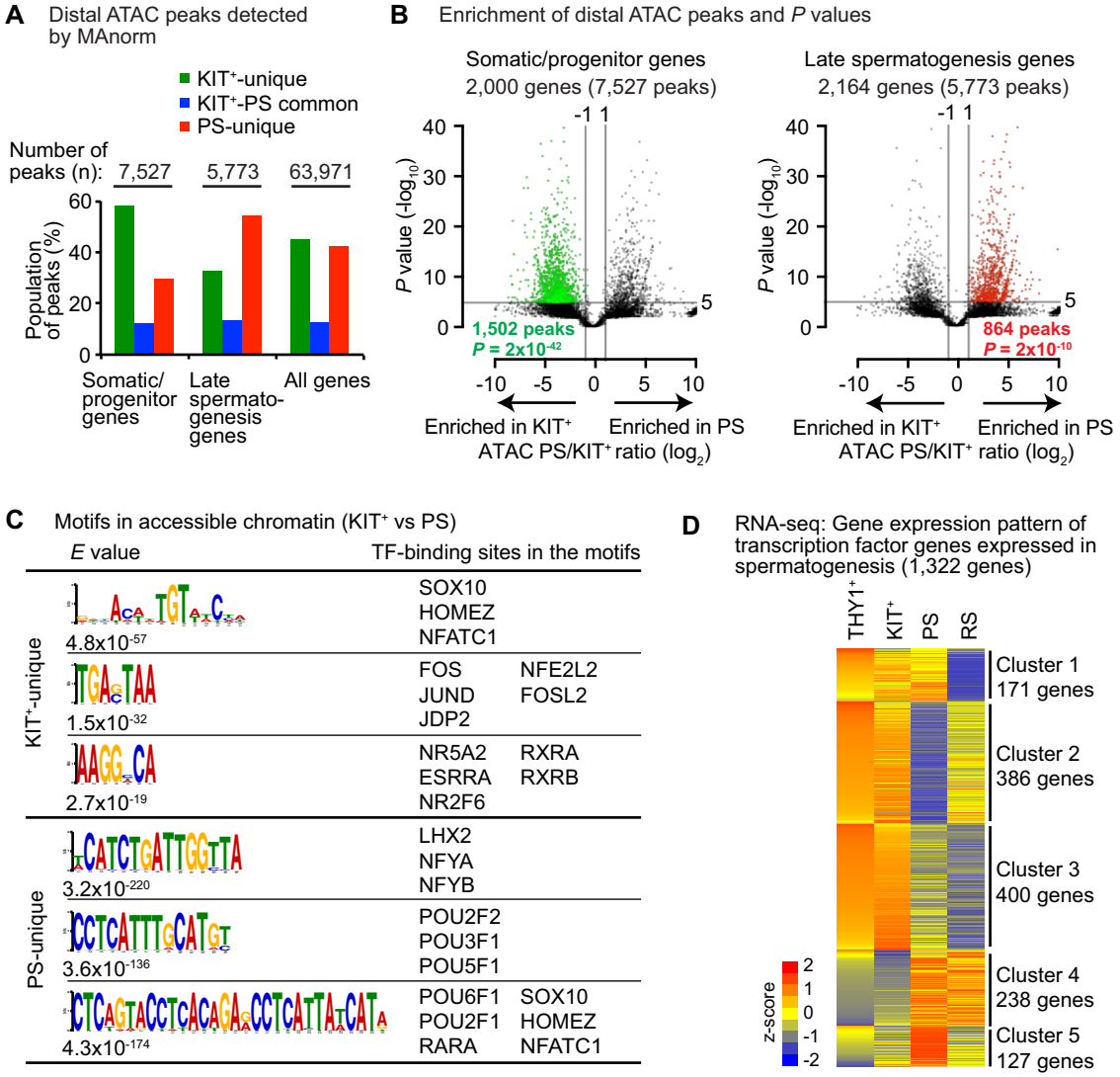

Figure 4. Identification of distal gene regulatory regions during the mitosis-to-meiosis transition. (**A**) Percentage distribution of distal ATAC peaks outside ±1 kb of TSSs detected by MAnorm between KIT$^+$ spermatogonia and PS. (**B**) Volcano plot for enrichment and *P*-values of distal ATAC peaks outside ±1 kb of TSSs during the transition from KIT$^+$ spermatogonia to PS. Peaks were detected by MAnorm, shown for those neighboring somatic/progenitor genes (left panel) and for those neighboring late spermatogenesis genes (right panel). Differential regions ($P < 1 \times 10^{-5}$, hypergeometric probability test; fold changes >2) are shown in green or red along with *P*-values from hypergeometric probability tests. (**C**) Motif analysis of ATAC peaks for putative transcription factor (TF)-binding sites. A total of 3000 peaks (±250 bp from summit) were selected from the lowest *P*-values for KIT$^+$ spermatogonia- and PS-unique peaks and analyzed by MEME-ChIP. (**D**) Heatmap of TF gene expression during spermatogenesis detected by RNA-seq. All TF genes categorized in the Gene Ontology (GO) database were analyzed. TF genes expressed in least at one of the four stages were included.

diately before meiosis and is involved in spermatogenesis (57,58). RNA-seq analysis revealed that POU family TF expression changes radically during spermatogenesis: While *Pou2f1* (*Oct1*), *Pou3f1* (*Oct6*), *Pou4f1* and *Pou5f1* (*Oct3/4*) are highly expressed in THY1$^+$ and KIT$^+$ spermatogonia, *Pou2f2* (*Oct2*), *Pou5f2,* and *Pou6f1* are highly expressed in PS (Supplementary Figure S6B). These results suggest that distal accessible chromatin is temporarily formed in PS to facilitate the recruitment of TFs that facilitate a gene expression program specific to meiosis.

Additional analyses of distal accessible chromatin revealed unique regulatory elements in the other critical transitions of spermatogenesis. Because chromatin compaction occurs during spermatogonial differentiation (THY1$^+$ to KIT$^+$ spermatogonia) and the meiosis-to-postmeiosis transition (PS to RS), we identified regions associated with TF-binding motifs in accessible chromatin that are subsequently closed during spermatogenesis. In THY1$^+$ spermatogonia, motifs for the FOX, FOS and JUN family TFs are open. Although many motifs remain accessible in KIT$^+$ spermatogonia and are closed off in PS (Figure 4C), a small portion is closed off in KIT$^+$ spermatogonia (Supplementary Figure S7A). Likewise, we detected accessible chromatin in PS that is subsequently closed in RS; associated motifs tend to be long and include binding sites for POU and FOX family TFs (Supplementary Figure S7B).

Because genome-wide gene expression changes dynamically during spermatogenesis, we predicted that expres-

sion changes in TF genes occur during spermatogenesis. Through RNA-seq analysis, we found that 1322 TF genes were expressed during spermatogenesis in at least one of the following stages: THY1$^+$ spermatogonia, KIT$^+$ spermatogonia, PS and RS; we categorized these TF genes into five clusters by k-means clustering (Figure 4D). Aside from the TF genes of Cluster 1 (171 genes), which are downregulated in RS, all TF genes demonstrate a notable expression change in the mitosis-to-meiosis transition (i.e. between KIT$^+$ spermatogonia and PS). TF genes in Cluster 2 (386 genes) and Cluster 3 (400 genes) are highly expressed in spermatogonia, but are downregulated in PS. TF genes in Cluster 4 (238 genes) and Cluster 5 (127 genes) are not highly expressed in spermatogonia, but are highly expressed in PS. These results suggest that, as genome-wide gene expression changes are taking place, a large and shifting repertoire of TFs are expressed during spermatogenesis.

Since distal ATAC peaks contain TF-binding sites, we reasoned that the distribution of these TF-binding sites, and thus accessible chromatin, is critical for spermatogenesis-specific gene regulation. Therefore, we sought to determine the positions of accessible chromatin relative to TSSs. To this end, we analyzed our ATAC-seq datasets with the Genomic Regions Enrichment of Annotations Tool (GREAT), which assigns biological meaning to a set of non-coding genomic regions by analyzing the annotations of nearby genes (32). We found that most accessible chromatin is located in the range of 5–500 kb from TSSs in KIT$^+$ spermatogonia and PS (Supplementary Figure S7C and D). Accessible chromatin common to KIT$^+$ spermatogonia and PS tended to be closer to TSSs, with a majority of sites in the range of 5–50 kb. Accessible chromatin unique to either KIT$^+$ spermatogonia or PS tended to be found in the range of 50–500 kb from TSSs. Therefore, it is conceivable that transcriptional changes during spermatogenesis are regulated by long-range *cis* regulatory elements.

SCML2 regulates genome-wide chromatin compaction in round spermatids

Next, we sought to determine the regulatory mechanisms for accessible chromatin during spermatogenesis. During stages of late spermatogenesis, such as PS and RS, SCML2, a germline-specific Polycomb protein, suppresses expression of somatic/progenitor genes and activates late spermatogenesis genes (14). In general, Polycomb proteins regulate heritable gene silencing and define cell-type specific gene expression, thereby defining cellular identity (59–61). Accordingly, SCML2 has vital functions for the unique, dynamic gene expression programs of spermatogenesis. Therefore, we hypothesized that SCML2 regulates chromatin accessibility during spermatogenesis to facilitate germline-specific gene expression. To test this hypothesis, we performed ATAC-seq of germ cells from each representative stage of spermatogenesis using *Scml2* knockout (KO) mice, and we compared ATAC-seq peaks between that of wild-type and *Scml2*-KO mice by MAnorm analysis (Figure 5A). Following the approach we used with wild-type samples, we carried out ATAC-seq for two independent biological replicates for each stage of spermatogenesis in *Scml2*-KO testes. In THY1$^+$ and KIT$^+$ spermatogonia, we detected little change in chromatin accessibility between wild-type and *Scml2*-KO. However, we identified 7942 peaks unique to wild-type PS, suggesting that SCML2 promotes the formation of open chromatin in PS. By comparison, we detected 2959 peaks unique to PS of *Scml2*-KO, indicating that SCML2 is also associated with the compaction/closure of accessible chromatin.

Remarkably, in RS of the *Scml2*-KO, we identified 34 407 unique peaks in intergenic or intronic regions (Figure 5A). Because a large amount of accessible chromatin in intergenic and intronic regions is closed during the transition from wild-type PS to RS (Figure 3A), we sought to determine whether SCML2 is involved in this step. We found that, among the 13 424 ATAC peaks unique to PS detected by MAnorm analysis of wild-type PS and RS (Figure 3A), most of these peaks remained open in RS of *Scml2*-KO mice while, for the most part, these peaks did not change in PS of *Scml2*-KO mice (Figure 5B). Therefore, we conclude that SCML2 is involved in the compaction/closure of accessible chromatin in the transition from PS to RS.

De novo formation of accessible chromatin during meiotic sex chromosome inactivation

Unique within the genome-wide dynamics of chromatin accessibility, we observed that accessible chromatin is increased at the transcriptionally silenced sex chromosomes in PS (Figure 1). The sex chromosomes are silenced during meiosis in a process known as meiotic sex chromosome inactivation (MSCI). MSCI is directed by DNA damage response pathways (62–64), which subject the sex chromosomes to epigenetic regulation distinct from autosomes. Therefore, we sought to elucidate the dynamics of accessible chromatin at the sex chromosomes before and after MSCI.

In spermatogonia, accessible chromatin at the sex chromosomes was modestly reduced from THY1$^+$ to KIT$^+$ spermatogonia (Figure 6A). This decrease is similar to that at autosomes from THY1$^+$ to KIT$^+$ spermatogonia, suggesting that autosomes and sex chromosomes are subject to similar forms of regulation during spermatogonial differentiation. Strikingly, we observed an extensive change in chromatin accessibility at the sex chromosomes from KIT$^+$ spermatogonia to PS (Figure 6A). While accessible chromatin in promoters was largely consistent from KIT$^+$ spermatogonia to PS at the sex chromosomes, a majority of accessible chromatin in intronic and intergenic regions of KIT$^+$ spermatogonia was closed in PS as is the case with the autosomes. Notably, in spite of the transcriptional silencing associated with MSCI, a large number of unique ATAC peaks appeared at the sex chromosomes. Therefore, MSCI does not accompany chromatin compaction, a form of chromatin regulation typically associated with transcriptional silencing, and instead promotes the *de novo* formation of accessible chromatin in intergenic and intronic regions. Indeed, this is consistent with previous cytological observations: Although the sex chromosomes form a subnuclear, transcriptionally silent compartment in the mid pachytene stage—termed the XY body—the initial stage of the XY body is not DAPI-dense. The XY body becomes a DAPI-dense heterochromatin compartment after the transition of the pachytene stage into the subsequent diplotene

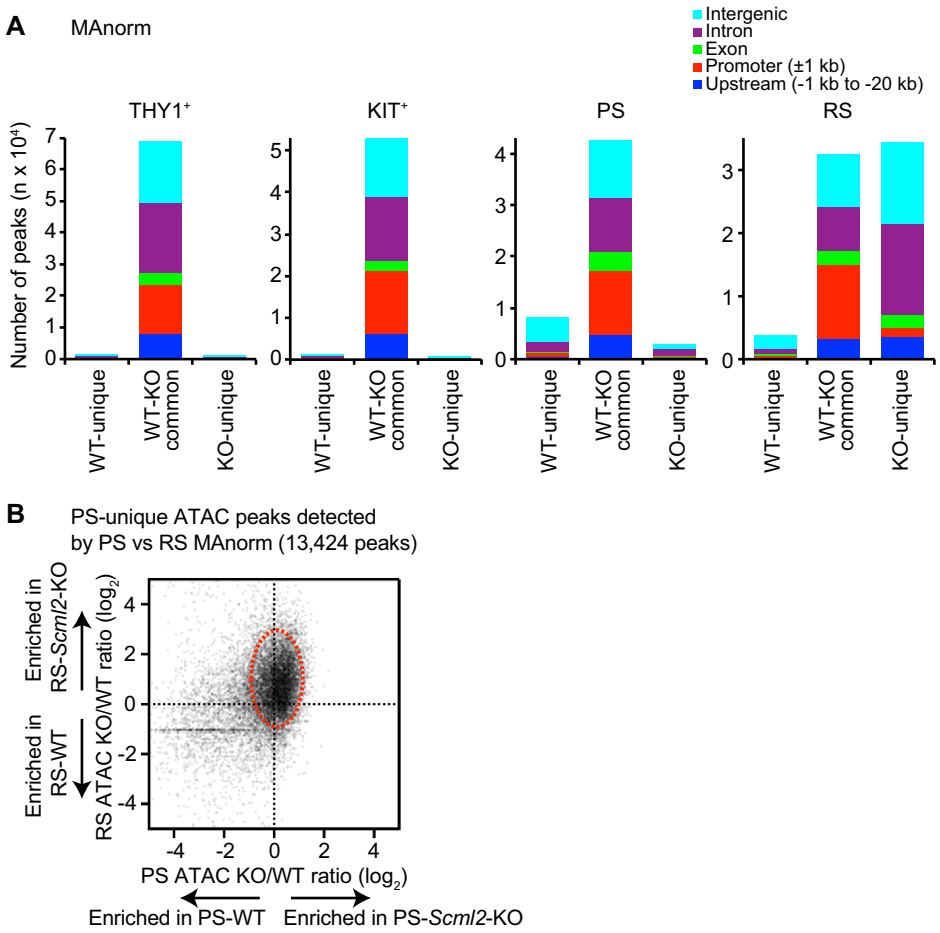

Figure 5. SCML2-dependent regulation of accessible chromatin in late spermatogenesis. (**A**) MAnorm analysis of ATAC peaks in each representative stage of spermatogenesis between wild-type and *Scml2*-KO mice. The genomic distribution of each peak is shown with colored bars. (**B**) Enrichment analysis of PS-unique ATAC peaks detected by MAnorm analysis between PS and RS (total 13 424 peaks). For each peak, the log2 ratio between WT and *Scml2*-KO in PS or RS is shown.

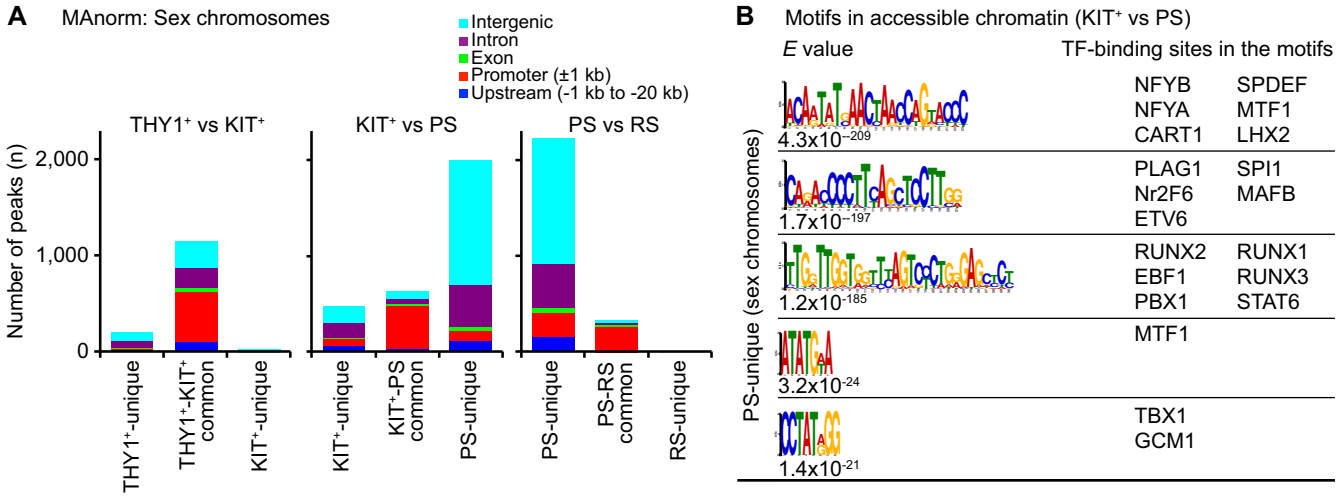

Figure 6. *De novo* formation of accessible chromatin during meiotic sex chromosome inactivation. (**A**) MAnorm analysis of ATAC peaks at the sex chromosomes at each transition during spermatogenesis. The genomic distribution of each peak is shown with colored bars. (**B**) Motif analysis of ATAC peaks for putative TF-binding sites on the sex chromosomes in PS. A total of 3000 peaks (±250 bp from summit) were selected from the lowest *E*-values for PS-unique peaks and analyzed by MEME-ChIP.

stage (11). Notably, this PS-specific accessible chromatin was closed in RS (Figure 6A). Therefore, PS-specific accessible chromatin is a unique feature of the sex chromosomes during meiosis.

Since open chromatin contains regulatory elements, we sought to determine if PS-specific peaks of accessible chromatin at the sex chromosomes have common motifs for TF binding. To this end, we performed motif analysis with MEME-ChIP (48). We identified consensus sequences for TF binding at the sex chromosomes in PS (Figure 6B). These consensus sequences are distinct from those found in genome-wide accessible chromatin (Figure 4C). The motif with the lowest *E*-value (*E*-value = 4.3×10^{-209}) contains binding sites for NFYA and NFYB, which are likely to be involved in meiosis-specific gene regulation (55). In addition to relatively long motifs, we also found the short motifs ATATGxA and CCTATxGG, which contain binding sites for MTF1, TBX1 and GCM1; however, the functions of these TFs in spermatogenesis are unknown. Since near-complete transcriptional silencing occurs in MSCI, the specific functions of exposed TF-binding motifs at the sex chromosome are enigmatic. It is possible that the motifs have functions for gene activation in later stages. Following meiosis, sex chromosome inactivation is largely maintained into RS via a heterochromatic, subnuclear compartment termed postmeiotic sex chromatin (PMSC) (11); however, a subset of genes required for male reproduction escape silencing for specific activation in RS (65–67). Therefore, these consensus sequences could function to prepare gene activation in later stages.

SCML2 is required for *de novo* formation of accessible chromatin during meiotic sex chromosome inactivation

During meiosis, SCML2 accumulates on the sex chromosomes downstream of DNA damage response pathways (14). In spermatogenesis, SCML2 has a role on sex chromosomes distinct from its role on autosomes (14), so we sought to determine the function of SCML2 in the regulation of accessible chromatin at sex chromosomes (Figure 7A). There was almost no change in accessible chromatin in THY1$^+$ and KIT$^+$ spermatogonia between wild-type and *Scml2*-KO mice. However, the PS-specific accessible chromatin of wild-type mice was not detected in PS of *Scml2*-KO. Furthermore, there was no significant change in RS between wild-type and *Scml2*-KO mice, consistent with the closure of accessible chromatin at the sex chromosomes in wild-type RS. To independently confirm the SCML2-dependent formation of PS-specific accessible chromatin, we tested the function of SCML2 on chromatin accessibility in the mitosis-to-meiosis transition. We identified 28 796 ATAC peaks unique to PS by MAnorm analysis between wild-type KIT$^+$ spermatogonia and wild-type PS (Figure 3A). Among them, 2003 peaks were sex chromosome-specific ATAC peaks. These peaks are detected exclusively in wild-type, but not *Scml2*-KO, mice (Figure 7B). These results indicate that SCML2 is required for the *de novo* formation of PS-specific accessible chromatin at the sex chromosomes.

DISCUSSION

In this study, we describe the genome-wide landscape of accessible chromatin during spermatogenesis, and we reveal the dynamic reorganization of open chromatin during spermatogenesis. Chromatin reorganization underlies genome-wide gene expression changes, which in turn influence the production of functional sperm. The most striking change in accessible chromatin occurs in intergenic and intronic regions at the mitosis-to-meiosis transition (KIT$^+$ spermatogonia to PS). At that time, the vast majority of accessible chromatin in intergenic and intronic regions in KIT$^+$ spermatogonia are closed in PS, while a large amount of accessible chromatin in intergenic and intronic regions is established *de novo* in PS. We also show that this dynamic reorganization of open chromatin accompanies a genome-wide transcriptional change, when thousands of somatic/progenitor genes are suppressed and thousands of late spermatogenesis genes are activated (14,15), leading to high transcriptome complexity in spermatogenesis (3). Furthermore, our work supports the association of open chromatin with transcription, as opposed to other events in male germ cells, in the following ways: (i) accessible chromatin is largely independent of recombination hotspot remnants, and (ii) accessible chromatin contains stage-specific putative TF-binding motifs. Therefore, our data unravel the existence of two major types of open chromatin during spermatogenesis: (i) open chromatin that represents a gene expression program unique to mitotically proliferating progenitor cells (somatic/progenitor types, i.e. mitotic type), and (ii) open chromatin that represents a gene expression program specific to the stages of late spermatogenesis, including PS and RS (late spermatogenesis types, i.e. meiosis type) (Figure 7C).

Differentiation processes, such as spermatogonial differentiation (THY1$^+$ to KIT$^+$ spermatogonia) and the meiosis-to-postmeiosis transition (PS to RS), involve chromatin closure without the *de novo* formation of accessible chromatin. Therefore, open chromatin in KIT$^+$ is a remnant of that in THY1$^+$, and open chromatin in RS is a remnant of that in PS. These findings distinguish two types of chromatin arrangement during spermatogenesis: (i) chromatin reorganization via the *de novo* formation of open chromatin during the mitosis-to-meiosis transition, and (ii) differentiation marked by chromatin closure. Of particular interest, we have revealed genome-wide changes in chromatin structure during the mitosis-to-meiosis transition at both autosomes and the sex chromosomes, which facilitate the gene expression programs of spermatogenesis (Figure 7C). Because post-transcriptional regulation is a unique feature of late spermatogenesis, facilitating the storage of mRNAs that ensure the timely expression of proteins (68), an important future direction is to unravel how dynamic changes in open chromatin prepare a repertoire of stored RNAs and influence their post-transcriptional regulation.

An intriguing feature of accessible chromatin during spermatogenesis is its relative stability in promoter regions despite the global reorganization of accessible chromatin in intergenic and intronic regions. Although there is a modest reorganization during spermatogenesis, somatic/progenitor genes retain accessible chromatin in

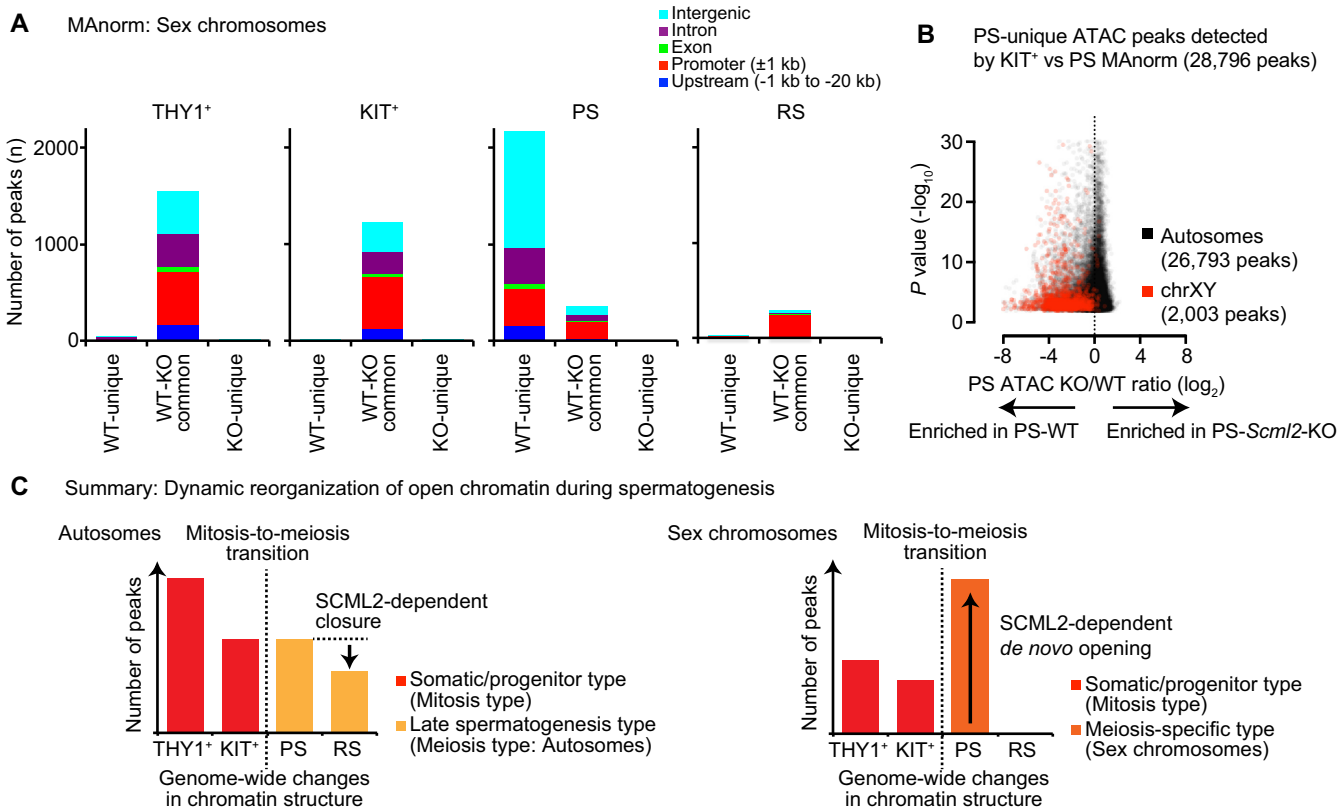

Figure 7. SCML2 is required for *de novo* formation of accessible chromatin during meiotic sex chromosome inactivation and a summary. (**A**) MAnorm analysis of ATAC peaks at the sex chromosomes in each representative stage of spermatogenesis between wild-type and *Scml2*-KO mice. The genomic distribution of each peak is shown with colored bars. (**B**) Enrichment analysis of PS-unique ATAC peaks detected by MAnorm analysis between KIT$^+$ spermatogonia and PS (total 28,796 peaks). For each peak, the log2 ratio between WT and *Scml2*-KO in PS is shown. (**C**) Schematic showing the summary of dynamic reorganization of accessible chromatin at intergenic and intronic regions during spermatogenesis. At autosomes, a large part of accessible chromatin is reorganized during the mitosis-to-meiosis transition, and SCML2 is involved in the closure of accessible chromatin during the transition between PS and RS. On the other hand, at the sex chromosomes, there is *de novo* formation of accessible chromatin during meiosis. This process is regulated by SCML2.

promoter regions after suppression in PS and RS, while late spermatogenesis genes already have accessible chromatin in promoter regions in spermatogonia. This feature may reflect the unipotent nature of male germ cells. Our previous study demonstrated that late spermatogenesis genes are poised for activation in the spermatogonial stem cell stage, while somatic/progenitor genes retain bivalent domains (H3K4me2/3 and H3K27me3) in late spermatogenesis, presumably to recover totipotency after fertilization (15). Because open chromatin at TSSs in RS is maintained at H3K4me3-enriched promoters in sperm, the stable open chromatin at TSSs potentially persists into early embryos. Therefore, germ cells are ready to facilitate the shifting, essential gene expression programs of various stages while still guarding the ability to recover totipotency after fertilization. The relative stability of accessible chromatin in promoter regions may be related to the unidirectional differentiation of germ cells. In turn, we infer that the accessible chromatin in intergenic and intronic regions functions in gene expression changes due to its dynamic reorganization. Curiously, the histone variant H3.3 was found to predominate sites of histone retention in sperm (25). Furthermore, testis-specific H3T, another variant of H3, is required for spermatogenesis (69). Therefore, it is an interesting possibility that these histone variants underlie unique chromatin features such as stable open chromatin in promoter regions to ensure the unidirectional differentiation of spermatogenesis.

In addition to these features, we identified a distinct feature of the sex chromosomes: the *de novo* formation of accessible chromatin in MSCI, suggesting that chromatin events are highly dynamic in spite of the transcriptional silencing of MSCI. In agreement with this dynamic chromatin feature, histone modifications are progressively established on the sex chromosomes during meiosis (11,70). Of note, a cascade of active epigenetic modifications, such as H4K20me1 and H3K4me2, are established on the sex chromosome during meiosis by the DNA damage response protein RNF8 (66), leading to the activation of male reproduction genes from the largely silent sex chromosomes, found within the heterochromatic PMSC structure in postmeiotic spermatids. Because the establishment of these active modifications in meiosis precedes gene activation, MSCI must prepare for gene activation in the postmeiotic stage. Therefore, one possible function of open chromatin in MSCI is to prepare gene activation for postmeiotic stages. Another possibility is that open chromatin at the sex chromosomes have meiotic functions *per se*, such as the establishment of

gene silencing. Further investigation is warranted to determine the functional roles of open chromatin in MSCI for gene activation from the heterochromatic PMSC structure in postmeiotic spermatids.

Finally, our study revealed distinct mechanisms for the regulation of chromatin accessibility between autosomes and sex chromosomes. While SCML2 promotes the *de novo* formation of accessible chromatin at the sex chromosomes during meiosis, SCML2 also promotes the closure of accessible chromatin at autosomes in RS (Figure 7C). This difference likely reflects two distinct functions for SCML2 that we previously described (14): on the sex chromosomes during meiosis, SCML2 removes ubiquitination of histone H2A at Lysine 119, a repressive modification mediated by PRC1, while also promoting the ubiquitination of histone H2A at Lysine 119 on autosomes. Because SCML2 is responsible for the suppression of somatic/progenitor genes, the activation of late spermatogenesis genes and efficient MSCI (14), the SCML2-dependent regulation of accessible chromatin is likely related to SCML2-dependent transcriptional regulation. Although we cannot exclude a possibility that SCML2's functions in earlier stages may indirectly influence the distribution of open chromatin that was observed in later postmeiotic spermatids, our results reveal critical functions of SCML2 for the organization of germline chromatin.

Together, our study presents a framework for chromatin dynamics at four representative stages of spermatogenesis. Datasets for these representative stages define the overall dynamics of open chromatin in spermatogenesis and detect possible regulatory elements for spermatogenesis-specific gene expression. This work will enable the further determination of chromatin mechanisms that facilitate spermatogenesis, a complex developmental process comprising many different substages, including those of spermatogonia, meiotic spermatocytes and postmeiotic spermatids. In addition, mitotic chromosomes undergo cycles of expansion and contraction with each mitotic division (71), and meiotic chromosomes undergo dynamic movement, including recombination, pairing and synapsis (72). Therefore, to capture chromosome movement and cell-to-cell variation during spermatogenesis, further characterizations of open chromatin in each substage, along with analyses of individual cells through single cell ATAC-seq (73), are warranted for future investigation.

AVAILABILITY

ATAC-seq datasets generated in this study were deposited to the NCBI Gene Expression Omnibus (GEO; https://www.ncbi.nlm.nih.gov/geo/) under accession number GSE102954.

SUPPLEMENTARY DATA

Supplementary Data are available at NAR Online.

ACKNOWLEDGEMENTS

We thank Andrey V. Kartashov for technical assistance and Katie Gerhardt for editing the manuscript.

Authors contribution: S.M. and S.H.N. designed the experiments; S.M. performed and interpreted most of the experiments; M.Y., K.G.A. and A.B. contributed bioinformatics data analysis with S.M.; S.M. and S.H.N. wrote the manuscript with all other authors.

FUNDING

March of Dimes Foundation [FY13–510 to S.H.N.]; National Institutes of Health [GM119134, HL098691 to A.B., GM098605, ES027117 to S.H.N.]. Funding for open access charge: National Institutes of Health [GM098605].
Conflict of interest statement. None declared.

REFERENCES

1. Ramskold,D., Wang,E.T., Burge,C.B. and Sandberg,R. (2009) An abundance of ubiquitously expressed genes revealed by tissue transcriptome sequence data. *PLoS Comput. Biol.*, **5**, e1000598.
2. Brawand,D., Soumillon,M., Necsulea,A., Julien,P., Csardi,G., Harrigan,P., Weier,M., Liechti,A., Aximu-Petri,A., Kircher,M. *et al.* (2011) The evolution of gene expression levels in mammalian organs. *Nature*, **478**, 343–348.
3. Soumillon,M., Necsulea,A., Weier,M., Brawand,D., Zhang,X., Gu,H., Barthes,P., Kokkinaki,M., Nef,S., Gnirke,A. *et al.* (2013) Cellular source and mechanisms of high transcriptome complexity in the mammalian testis. *Cell Rep.*, **3**, 2179–2190.
4. Griswold,M.D. (2016) Spermatogenesis: the commitment to meiosis. *Physiol. Rev.*, **96**, 1–17.
5. Kimmins,S. and Sassone-Corsi,P. (2005) Chromatin remodelling and epigenetic features of germ cells. *Nature*, **434**, 583–589.
6. Kota,S.K. and Feil,R. (2010) Epigenetic transitions in germ cell development and meiosis. *Dev. Cell*, **19**, 675–686.
7. Sasaki,H. and Matsui,Y. (2008) Epigenetic events in mammalian germ-cell development: reprogramming and beyond. *Nat. Rev. Genet.*, **9**, 129–140.
8. Schultz,N., Hamra,F.K. and Garbers,D.L. (2003) A multitude of genes expressed solely in meiotic or postmeiotic spermatogenic cells offers a myriad of contraceptive targets. *Proc. Natl. Acad. Sci. U.S.A.*, **100**, 12201–12206.
9. Khil,P.P., Smirnova,N.A., Romanienko,P.J. and Camerini-Otero,R.D. (2004) The mouse X chromosome is enriched for sex-biased genes not subject to selection by meiotic sex chromosome inactivation. *Nat. Genet.*, **36**, 642–646.
10. Shima,J.E., McLean,D.J., McCarrey,J.R. and Griswold,M.D. (2004) The murine testicular transcriptome: characterizing gene expression in the testis during the progression of spermatogenesis. *Biol. Reprod.*, **71**, 319–330.
11. Namekawa,S.H., Park,P.J., Zhang,L.F., Shima,J.E., McCarrey,J.R., Griswold,M.D. and Lee,J.T. (2006) Postmeiotic sex chromatin in the male germline of mice. *Curr. Biol.*, **16**, 660–667.
12. Chalmel,F., Rolland,A.D., Niederhauser-Wiederkehr,C., Chung,S.S., Demougin,P., Gattiker,A., Moore,J., Patard,J.J., Wolgemuth,D.J., Jegou,B. *et al.* (2007) The conserved transcriptome in human and rodent male gametogenesis. *Proc. Natl. Acad. Sci. U.S.A.*, **104**, 8346–8351.
13. Fallahi,M., Getun,I.V., Wu,Z.K. and Bois,P.R. (2010) A global expression switch marks pachytene initiation during mouse male meiosis. *Genes (Basel)*, **1**, 469–483.
14. Hasegawa,K., Sin,H.S., Maezawa,S., Broering,T.J., Kartashov,A.V., Alavattam,K.G., Ichijima,Y., Zhang,F., Bacon,W.C., Greis,K.D. *et al.* (2015) SCML2 establishes the male germline epigenome through regulation of histone H2A ubiquitination. *Dev. Cell*, **32**, 574–588.
15. Sin,H.S., Kartashov,A.V., Hasegawa,K., Barski,A. and Namekawa,S.H. (2015) Poised chromatin and bivalent domains facilitate the mitosis-to-meiosis transition in the male germline. *BMC Biol.*, **13**, 53.
16. Margolin,G., Khil,P.P., Kim,J., Bellani,M.A. and Camerini-Otero,R.D. (2014) Integrated transcriptome analysis of mouse spermatogenesis. *BMC Genomics*, **15**, 39.

17. Ball,R.L., Fujiwara,Y., Sun,F., Hu,J., Hibbs,M.A., Handel,M.A. and Carter,G.W. (2016) Regulatory complexity revealed by integrated cytological and RNA-seq analyses of meiotic substages in mouse spermatocytes. *BMC Genomics*, **17**, 628.
18. da Cruz,I., Rodriguez-Casuriaga,R., Santinaque,F.F., Farias,J., Curti,G., Capoano,C.A., Folle,G.A., Benavente,R., Sotelo-Silveira,J.R. and Geisinger,A. (2016) Transcriptome analysis of highly purified mouse spermatogenic cell populations: gene expression signatures switch from meiotic-to postmeiotic-related processes at pachytene stage. *BMC Genomics*, **17**, 294.
19. Hammoud,S.S., Low,D.H., Yi,C., Carrell,D.T., Guccione,E. and Cairns,B.R. (2014) Chromatin and transcription transitions of mammalian adult germline stem cells and spermatogenesis. *Cell Stem Cell*, **15**, 239–253.
20. Buenrostro,J.D., Giresi,P.G., Zaba,L.C., Chang,H.Y. and Greenleaf,W.J. (2013) Transposition of native chromatin for fast and sensitive epigenomic profiling of open chromatin, DNA-binding proteins and nucleosome position. *Nat. Methods*, **10**, 1213–1218.
21. Bellve,A.R. (1993) Purification, culture, and fractionation of spermatogenic cells. *Methods Enzymol.*, **225**, 84–113.
22. Zhang,J., Bonasio,R., Strino,F., Kluger,Y., Holloway,J.K., Modzelewski,A.J., Cohen,P.E. and Reinberg,D. (2013) SFMBT1 functions with LSD1 to regulate expression of canonical histone genes and chromatin-related factors. *Genes Dev.*, **27**, 749–766.
23. Smagulova,F., Brick,K., Pu,Y., Camerini-Otero,R.D. and Petukhova,G.V. (2016) The evolutionary turnover of recombination hot spots contributes to speciation in mice. *Genes Dev.*, **30**, 266–280.
24. Walker,M., Billings,T., Baker,C.L., Powers,N., Tian,H., Saxl,R.L., Choi,K., Hibbs,M.A., Carter,G.W., Handel,M.A. *et al.* (2015) Affinity-seq detects genome-wide PRDM9 binding sites and reveals the impact of prior chromatin modifications on mammalian recombination hotspot usage. *Epigenet. Chromatin*, **8**, 31.
25. Erkek,S., Hisano,M., Liang,C.Y., Gill,M., Murr,R., Dieker,J., Schubeler,D., van der Vlag,J., Stadler,M.B. and Peters,A.H. (2013) Molecular determinants of nucleosome retention at CpG-rich sequences in mouse spermatozoa. *Nat. Stuct. Mol. Biol.*, **20**, 868–875.
26. Kartashov,A.V. and Barski,A. (2015) BioWardrobe: an integrated platform for analysis of epigenomics and transcriptomics data. *Genome Biol.*, **16**, 158.
27. Langmead,B., Trapnell,C., Pop,M. and Salzberg,S.L. (2009) Ultrafast and memory-efficient alignment of short DNA sequences to the human genome. *Genome Biol.*, **10**, R25.
28. Zhang,Y., Liu,T., Meyer,C.A., Eeckhoute,J., Johnson,D.S., Bernstein,B.E., Nusbaum,C., Myers,R.M., Brown,M., Li,W. *et al.* (2008) Model-based analysis of ChIP-Seq (MACS). *Genome Biol.*, **9**, R137.
29. Shao,Z., Zhang,Y., Yuan,G.C., Orkin,S.H. and Waxman,D.J. (2012) MAnorm: a robust model for quantitative comparison of ChIP-Seq data sets. *Genome Biol.*, **13**, R16.
30. Machanick,P. and Bailey,T.L. (2011) MEME-ChIP: motif analysis of large DNA datasets. *Bioinformatics*, **27**, 1696–1697.
31. Karolchik,D., Hinrichs,A.S., Furey,T.S., Roskin,K.M., Sugnet,C.W., Haussler,D. and Kent,W.J. (2004) The UCSC Table Browser data retrieval tool. *Nucleic Acids Res.*, **32**, D493–D496.
32. McLean,C.Y., Bristor,D., Hiller,M., Clarke,S.L., Schaar,B.T., Lowe,C.B., Wenger,A.M. and Bejerano,G. (2010) GREAT improves functional interpretation of cis-regulatory regions. *Nat. Biotechnol.*, **28**, 495–501.
33. Dobin,A., Davis,C.A., Schlesinger,F., Drenkow,J., Zaleski,C., Jha,S., Batut,P., Chaisson,M. and Gingeras,T.R. (2013) STAR: ultrafast universal RNA-seq aligner. *Bioinformatics*, **29**, 15–21.
34. Meyer,L.R., Zweig,A.S., Hinrichs,A.S., Karolchik,D., Kuhn,R.M., Wong,M., Sloan,C.A., Rosenbloom,K.R., Roe,G., Rhead,B. *et al.* (2013) The UCSC Genome Browser database: extensions and updates 2013. *Nucleic Acids Res.*, **41**, D64–D69.
35. Love,M.I., Huber,W. and Anders,S. (2014) Moderated estimation of fold change and dispersion for RNA-seq data with DESeq2. *Genome Biol.*, **15**, 550.
36. Turner,J.M., Mahadevaiah,S.K., Ellis,P.J., Mitchell,M.J. and Burgoyne,P.S. (2006) Pachytene asynapsis drives meiotic sex chromosome inactivation and leads to substantial postmeiotic repression in spermatids. *Dev. Cell*, **10**, 521–529.
37. Bernstein,B.E., Mikkelsen,T.S., Xie,X., Kamal,M., Huebert,D.J., Cuff,J., Fry,B., Meissner,A., Wernig,M., Plath,K. *et al.* (2006) A bivalent chromatin structure marks key developmental genes in embryonic stem cells. *Cell*, **125**, 315–326.
38. Azuara,V., Perry,P., Sauer,S., Spivakov,M., Jorgensen,H.F., John,R.M., Gouti,M., Casanova,M., Warnes,G., Merkenschlager,M. *et al.* (2006) Chromatin signatures of pluripotent cell lines. *Nat. Cell Biol.*, **8**, 532–538.
39. Voigt,P., Tee,W.W. and Reinberg,D. (2013) A double take on bivalent promoters. *Genes Dev.*, **27**, 1318–1338.
40. Brykczynska,U., Hisano,M., Erkek,S., Ramos,L., Oakeley,E.J., Roloff,T.C., Beisel,C., Schubeler,D., Stadler,M.B. and Peters,A.H. (2010) Repressive and active histone methylation mark distinct promoters in human and mouse spermatozoa. *Nat. Struct. Mol. Biol.*, **17**, 679–687.
41. Lesch,B.J., Dokshin,G.A., Young,R.A., McCarrey,J.R. and Page,D.C. (2013) A set of genes critical to development is epigenetically poised in mouse germ cells from fetal stages through completion of meiosis. *Proc. Natl. Acad. Sci. U.S.A.*, **110**, 16061–16066.
42. Hammoud,S.S., Nix,D.A., Zhang,H., Purwar,J., Carrell,D.T. and Cairns,B.R. (2009) Distinctive chromatin in human sperm packages genes for embryo development. *Nature*, **460**, 473–478.
43. Sachs,M., Onodera,C., Blaschke,K., Ebata,K.T., Song,J.S. and Ramalho-Santos,M. (2013) Bivalent chromatin marks developmental regulatory genes in the mouse embryonic germline in vivo. *Cell Rep.*, **3**, 1777–1784.
44. Lesch,B.J. and Page,D.C. (2014) Poised chromatin in the mammalian germ line. *Development*, **141**, 3619–3626.
45. Lesch,B.J., Silber,S.J., McCarrey,J.R. and Page,D.C. (2016) Parallel evolution of male germline epigenetic poising and somatic development in animals. *Nat. Genet.*, **48**, 888–894.
46. Khil,P.P., Smagulova,F., Brick,K.M., Camerini-Otero,R.D. and Petukhova,G.V. (2012) Sensitive mapping of recombination hotspots using sequencing-based detection of ssDNA. *Genome Res.*, **22**, 957–965.
47. Wu,J., Huang,B., Chen,H., Yin,Q., Liu,Y., Xiang,Y., Zhang,B., Liu,B., Wang,Q., Xia,W. *et al.* (2016) The landscape of accessible chromatin in mammalian preimplantation embryos. *Nature*, **534**, 652–657.
48. Ma,W., Noble,W.S. and Bailey,T.L. (2014) Motif-based analysis of large nucleotide data sets using MEME-ChIP. *Nat. Protoc.*, **9**, 1428–1450.
49. Bailey,T.L., Boden,M., Buske,F.A., Frith,M., Grant,C.E., Clementi,L., Ren,J., Li,W.W. and Noble,W.S. (2009) MEME SUITE: tools for motif discovery and searching. *Nucleic Acids Res.*, **37**, W202–W208.
50. Polanco,J.C., Wilhelm,D., Davidson,T.L., Knight,D. and Koopman,P. (2010) Sox10 gain-of-function causes XX sex reversal in mice: implications for human 22q-linked disorders of sex development. *Hum. Mol. Genet.*, **19**, 506–516.
51. Kubo,N., Toh,H., Shirane,K., Shirakawa,T., Kobayashi,H., Sato,T., Sone,H., Sato,Y., Tomizawa,S., Tsurusaki,Y. *et al.* (2015) DNA methylation and gene expression dynamics during spermatogonial stem cell differentiation in the early postnatal mouse testis. *BMC Genomics*, **16**, 624.
52. Milde-Langosch,K. (2005) The Fos family of transcription factors and their role in tumourigenesis. *Eur. J. Cancer*, **41**, 2449–2461.
53. Ng,J.H., Kumar,V., Muratani,M., Kraus,P., Yeo,J.C., Yaw,L.P., Xue,K., Lufkin,T., Prabhakar,S. and Ng,H.H. (2013) In vivo epigenomic profiling of germ cells reveals germ cell molecular signatures. *Dev. Cell*, **24**, 324–333.
54. Gely-Pernot,A., Raverdeau,M., Teletin,M., Vernet,N., Feret,B., Klopfenstein,M., Dennefeld,C., Davidson,I., Benoit,G., Mark,M. *et al.* (2015) Retinoic acid receptors control spermatogonia cell-fate and induce expression of the SALL4A transcription factor. *PLoS Genet.*, **11**, e1005501.
55. Hou,Y., Yuan,J., Zhou,X., Fu,X., Cheng,H. and Zhou,R. (2012) DNA demethylation and USF regulate the meiosis-specific expression of the mouse Miwi. *PLoS Genet.*, **8**, e1002716.
56. Wu,X., Oatley,J.M., Oatley,M.J., Kaucher,A.V., Avarbock,M.R. and Brinster,R.L. (2010) The POU domain transcription factor POU3F1 is an important intrinsic regulator of GDNF-induced survival and self-renewal of mouse spermatogonial stem cells. *Biol. Reprod.*, **82**, 1103–1111.

57. Andersen,B., Pearse,R.V. 2nd, Schlegel,P.N., Cichon,Z., Schonemann,M.D., Bardin,C.W. and Rosenfeld,M.G. (1993) Sperm 1: a POU-domain gene transiently expressed immediately before meiosis I in the male germ cell. *Proc. Natl. Acad. Sci. U.S.A.*, **90**, 11084–11088.
58. Pearse,R.V. 2nd, Drolet,D.W., Kalla,K.A., Hooshmand,F., Bermingham,J.R. Jr and Rosenfeld,M.G. (1997) Reduced fertility in mice deficient for the POU protein sperm-1. *Proc. Natl. Acad. Sci. U.S.A.*, **94**, 7555–7560.
59. Aranda,S. and Mas,G. (2015) Regulation of gene transcription by Polycomb proteins. *Sci. Adv.*, **1**, e1500737.
60. Geisler,S.J. and Paro,R. (2015) Trithorax and Polycomb group-dependent regulation: a tale of opposing activities. *Development*, **142**, 2876–2887.
61. Laugesen,A. and Helin,K. (2014) Chromatin repressive complexes in stem cells, development, and cancer. *Cell Stem Cell*, **14**, 735–751.
62. Ichijima,Y., Ichijima,M., Lou,Z., Nussenzweig,A., Camerini-Otero,R.D., Chen,J., Andreassen,P.R. and Namekawa,S.H. (2011) MDC1 directs chromosome-wide silencing of the sex chromosomes in male germ cells. *Genes Dev.*, **25**, 959–971.
63. Ichijima,Y., Sin,H.S. and Namekawa,S.H. (2012) Sex chromosome inactivation in germ cells: emerging roles of DNA damage response pathways. *Cell Mol. Life Sci.*, **69**, 2559–2572.
64. Royo,H., Prosser,H., Ruzankina,Y., Mahadevaiah,S.K., Cloutier,J.M., Baumann,M., Fukuda,T., Hoog,C., Toth,A., de Rooij,D.G. *et al.* (2013) ATR acts stage specifically to regulate multiple aspects of mammalian meiotic silencing. *Genes Dev.*, **27**, 1484–1494.
65. Sin,H.S., Ichijima,Y., Koh,E., Namiki,M. and Namekawa,S.H. (2012) Human postmeiotic sex chromatin and its impact on sex chromosome evolution. *Genome Res.*, **22**, 827–836.
66. Sin,H.S., Barski,A., Zhang,F., Kartashov,A.V., Nussenzweig,A., Chen,J., Andreassen,P.R. and Namekawa,S.H. (2012) RNF8 regulates active epigenetic modifications and escape gene activation from inactive sex chromosomes in post-meiotic spermatids. *Genes Dev.*, **26**, 2737–2748.
67. Sin,H.S. and Namekawa,S.H. (2013) The great escape: Active genes on inactive sex chromosomes and their evolutionary implications. *Epigenetics*, **8**, 887–892.
68. Paronetto,M.P. and Sette,C. (2010) Role of RNA-binding proteins in mammalian spermatogenesis. *Int. J. Androl.*, **33**, 2–12.
69. Ueda,J., Harada,A., Urahama,T., Machida,S., Maehara,K., Hada,M., Makino,Y., Nogami,J., Horikoshi,N., Osakabe,A. *et al.* (2017) Testis-Specific Histone Variant H3t Gene Is Essential for Entry into Spermatogenesis. *Cell Rep.*, **18**, 593–600.
70. van der Heijden,G.W., Derijck,A.A., Posfai,E., Giele,M., Pelczar,P., Ramos,L., Wansink,D.G., van der Vlag,J., Peters,A.H. and de Boer,P. (2007) Chromosome-wide nucleosome replacement and H3.3 incorporation during mammalian meiotic sex chromosome inactivation. *Nat. Genet.*, **39**, 251–258.
71. Liang,Z., Zickler,D., Prentiss,M., Chang,F.S., Witz,G., Maeshima,K. and Kleckner,N. (2015) Chromosomes progress to metaphase in multiple discrete steps via global compaction/expansion cycles. *Cell*, **161**, 1124–1137.
72. Zickler,D. and Kleckner,N. (2015) Recombination, pairing, and synapsis of homologs during meiosis. *Cold Spring Harb. Perspect. Biol.*, **7**, a016626.
73. Buenrostro,J.D., Wu,B., Litzenburger,U.M., Ruff,D., Gonzales,M.L., Snyder,M.P., Chang,H.Y. and Greenleaf,W.J. (2015) Single-cell chromatin accessibility reveals principles of regulatory variation. *Nature*, **523**, 486–490.